IL NUOVO CIMENTO VOL. 20 D, N. 7-8 Luglio-Agosto 1998

Thermoelastic properties of Al:YIG ceramic systems (*)

N. SPARVIERI

Alenia, Research Department - Via Tiburtina km 12,4, 00131 Roma, Italy

(ricevuto il 23 Gennaio 1998; approvato il 19 Febbraio 1998)

Summary. — Interferometric thermal diffusivity measurements and elastic constants obtained by ultrasonic techniques on $Y_3Fe_{5-x}Al_xO_{12}$ (with $x = 0$, 0.4, 0.8, 1.1) ceramic samples are presented and discussed. The phonon mean free path is given as a function of x using the Boltzmann transport equation.

PACS 66.10.Cb – Diffusion and thermal diffusion.
PACS 62.30 – Mechanical and elastic waves; vibrations.
PACS 75.50.Gg – Ferrimagnetics.
PACS 01.30.Ee – Monographs and collections.

1. – Introduction

Some results of solid-state physics obtained on idealised models like the infinite crystal can be successfully applied, and with some modifications, also on granular material like ceramics. However, in such cases the observed physical properties, beyond the microscopic structure of the material, are affected also by the so-called mesoscopic structure, that is, mainly, the grain boundaries and porosity. One of the problems consists in understanding the contribution of such morphological structure on the diffusion of heat through the sample.

In this paper experimental results are presented of thermal diffusivity measurements obtained by a laser interferometric method on four ceramic samples of Al:YIG and at the same time elastic-constant measurements were obtained through ultrasonic techniques. It will be shown that at room temperature the phonon-phonon interaction is dominant and the extent of phonon scattering and the value of the mean free path should depend on the anharmonicity of the lattice vibrations.

2. – Experiments

The material under investigation is ceramic Yttrium Iron Garnet (YIG) with different concentrations of Al^{3+} substitutional ions [1]. Its preparation followed the standard ceramic technology available in the literature [2].

(*) In honour of Prof. Gianfranco Chiarotti on the occasion of his 70th birthday.

2·1. *Determination of the thermal diffusivity with the laser interferometric method.* – Measurements were taken using a Michelson interferometer showing the sample replacing one of the mirrors [3]. The surface of the sample was polished for reflection. A CO_2 laser beam of about 0.5 W heats the sample from behind.

A shutter placed on the laser beam establishes the exact starting time of heating and, in order to know the exact amount of energy transferred to the sample, the reflectivity of the surface was measured. We can estimate the value of the absorption coefficient ($\alpha = 10\ \mathrm{cm}^{-1}$) from the measured transmission coefficient and from that the exact amount of energy given to the sample can be obtained. For a more detailed discussion on the method, see ref. [3]. The heating mechanism can be summarised as follows. Before heating the sample, the He-Ne intensity at the photodetector is shown as

$$I_d = 2I_0(1 + \cos \Delta\varphi)\,, \tag{1}$$

where I_0 is the intensity of the laser beam and $\Delta\varphi$ is the phase shift between the two beams of the interferometer, that is

$$\Delta\varphi = \left(\frac{2\pi}{\lambda}\right)(d_1 - d_2) + \delta\,. \tag{2}$$

Here d_1 and d_2 are the two arm lengths, and δ is the phase shift due to the reflection at the sample surface. When the shutter of the CO_2 laser beam is open, the sample begins to heat and undergoes a thermal expansion. The thermal expansion produces a change Δl in the path of the laser beam reflected by the sample and therefore the phase shift between the two arms of the interferometer changes as shown

$$\delta = \left(\frac{2\pi}{\lambda}\right) 2\,\Delta l\,. \tag{3}$$

This phase shift produces a movement of the fringe pattern on the detector. Therefore the detector output has a temporal dependence which gives the temporal behaviour of Δl.

In order to calculate the thermal diffusivity, we start from the well-known solution of the one-dimensional lossless heat equation. For a semi-infinite slab

$$\Delta T_c = \Delta T_h \exp\left[\frac{-l^2}{4t_s\chi}\right], \tag{4}$$

ΔT_c and ΔT_h being the temperature increase on the back (cold) and front (hot) surface respectively, l is the sample length, t_s the diffusion time and χ the thermal diffusivity. The diffusion time in this experiment is defined as the delay between the time at which the heating beam is switched on and the time at which the first $\lambda/4$ fringe movement is detected.

We know that the thermal expansion coefficient, ΔT_c, is given as

$$\Delta T_c \approx \Delta T_h - 2\,\Delta l t_s \alpha\,, \tag{5}$$

Fig.

where α is the thermal expansion coefficient, ΔT_h is the rise in temperature due to the heating of the CO_2 laser and can be written as follows:

$$\Delta T_h = \frac{2P(1-R)}{c\varrho\chi\pi} \ln\left(\frac{4\chi t_s}{W_0^2} + 1\right) \tag{6}$$

for the case of a Gaussian heating source on a seminfinite slab where W_0 is the laser spot, P is the laser power, R is the surface reflectivity, ϱ is the density and c is the specific heat of the sample.

In the case where $4\chi t_s/W_0^2 \ll 1$, the above equation becomes

$$\Delta T_h = \frac{2P(1-R)}{c\varrho\pi} \frac{4t_s}{W_0^2} . \tag{7}$$

Therefore we can estimate the thermal diffusivity value

$$\chi = \frac{l^2}{4t_s} \ln\left(\frac{\Delta T_h}{\Delta T_c}\right). \tag{8}$$

With the method described above and after the realisation of a mirror-like surface for each Al-substituted sample, the results depicted in fig. 1 have been obtained [3].

Figure 2 shows the thermal diffusivity for the sample with $X = 1.1$ (the $Y_3Fe_{3.9}Al_{1.1}O_{12}$) as a function of the temperature.

In the graph discontinuity is clearly shown due to the specific heat at the Neel temperature ($\approx$ 393 K). This second-order phase transition implies that

$$\chi = \frac{Km}{\varrho T(\partial S/\partial T)} , \tag{9}$$

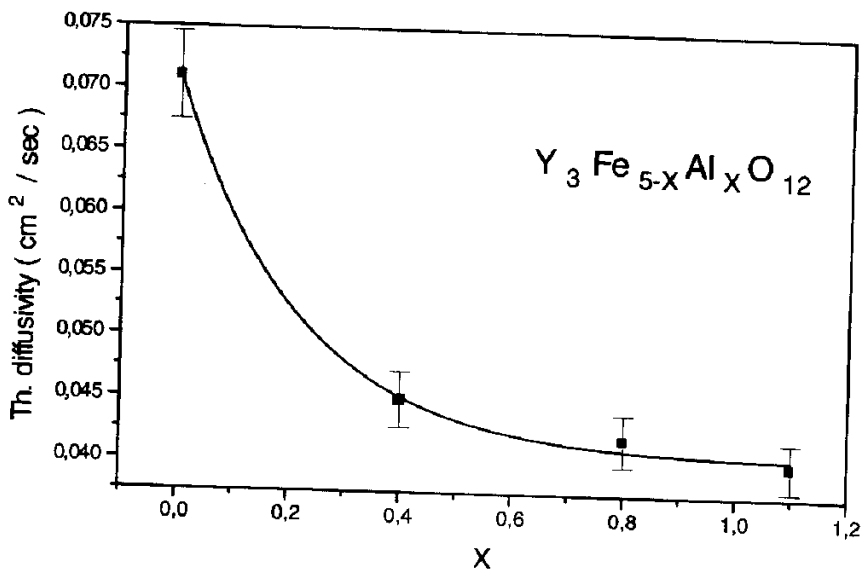

Fig. 1. – Thermal-diffusivity values measured as a function of the Al content.

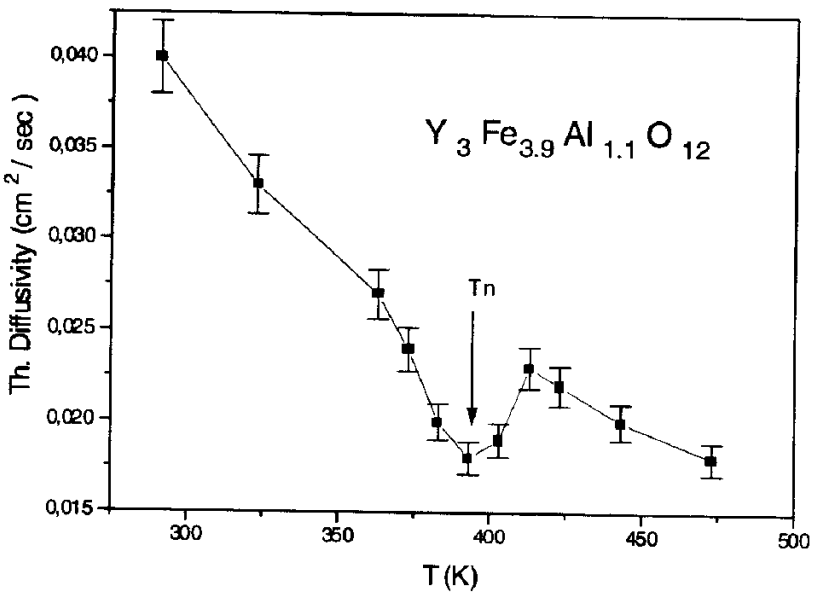

Fig. 2. – Thermal-diffusivity values measured as a function of the temperature in the sample with $X = 1.1$.

in which K is the thermal conductivity, m is the mass of the samples, ϱ is the mass density and S the entropy. The transition between a more ordered ferrimagnetic state to a less ordered paramagnetic state is associated to a variation in the entropy of the system.

2·2. *Elastic constants evaluation with the ultrasonic technique.* – The elastic properties of ceramic garnets have been studied by operating in a range of frequencies where the acoustic modes are almost exclusively elastic. In fact we assume that the acoustic frequencies of interest lie in the low megahertz range, so the exchange-free conditions are satisfied [4-7]. Under these conditions, the propagation medium can be considered purely elastic and isotropic. Two types of acoustic modes can propagate along the plate: Lamb and Love modes [7]. Lamb modes are polarised in the sagittal plane $(X_1 X_3)$ and consist of two longitudinal and two shear vertical partial waves coupled together.

The particle displacement components can be written in the form

$$u_i = \sum_{p=1}^{12} A_p a_i^p \exp[i\beta b^{(p)} x_3] \exp[i(\beta x_1 - \omega t)], \tag{10}$$

where β is the acoustic wave number of the mode, $\beta b^{(p)}$ the propagation constant along the normal to the plate of the p-th partial wave, whose amplitude and mechanical polarisation are given by A_p and $a_i^{(p)}$, respectively. Similar expressions can be written for the magnetic quantities associated with the acoustic field. The magnetoelastic coupling is fairly strong at the crossover points of the dispersion curves, where the uncoupled spin and elastic waves have the same wave number. For frequencies far away from the crossover values, the acoustic and magnetic waves are still coupled but

with a predominant elastic or magnetic character. In our case we have the following experimental conditions: $\omega = 3$ MHz, $h = 1$ mm; so we are in the range of almost pure elastic waves.

The dispersion relations, depending on both C_{11} and C_{44}, can be expressed in the form

$$(11)\quad \frac{\tan\left(\pi \frac{h}{\lambda}\sqrt{v^2 \frac{\varrho}{C_{44}} - 1}\right)}{\tan\left(\pi \frac{h}{\lambda}\sqrt{v^2 \frac{\varrho}{C_{11}} - 1}\right)} = -\left(\frac{\frac{4}{v^2}\frac{C_{44}}{\varrho}\sqrt{1 - \frac{1}{v^2}\frac{C_{44}}{\varrho}}\sqrt{\frac{C_{44}}{C_{11}} - \frac{1}{v_2}\frac{C_{44}}{\varrho}}}{\left(\frac{2}{v^2}\frac{C_{44}}{\varrho} - 1\right)^2}\right)^{\pm 1},$$

where the plus or minus sign of the exponent on the right-hand side of eq. (11) refers, respectively, to the symmetric or antisymmetric modes. Love modes, polarised along the X_2 direction, consist of two shear horizontal partial waves. Their phase velocity is related to the elastic constant C_{44} by the dispersion relations

$$(12)\quad \frac{\varrho}{C_{44}} = \frac{1}{v^2}\left(1 + \frac{n}{2(h/\lambda)}\right)^2,$$

with $n = 0, 1, 2, \ldots$.

Acoustic waves were generated and detected by means of meanderline transducers, configured by standard photolithographic techniques. The transducers consist of 11 meanders with a spatial periodicity $\lambda = 0.6$ mm and an electrode length of 4 mm. Two transducers, 24 mm apart were used for each sample, resulting in an acoustic delay line. Meanderline transducers are effective in generating and detecting both Lamb and Love waves, provided that the bias magnetic field is parallel or orthogonal to the acoustic propagation direction [8, 9].

All the modes having a wavelength λ equal to the period of the transducer can be generated and detected [10]. The two independent elastic constants of the material to be determined are C_{11} and C_{44}. They are related to the wavelength and velocity of the acoustic modes by the dispersion relations given in eqs. (11) and (12). Measurements of the frequency of the acoustic modes were performed by means of an HP 8753A network analyser. Firstly the Love modes were analysed, in order to evaluate the C_{44} constant [10]. In each sample the frequency corresponding to the first three modes was measured, and the experimental data processed according to the procedure outlined in the previous, in order to minimise the experimental error. A similar analysis, performed on the first three Lamb modes, allowed us the evaluation of the C_{11} constant. The measured elastic constants C_{11} and C_{44} of the four samples analysed are shown in fig. 3. The values relative to undoped YIG ceramic agree fairly well with those calculated by the single crystal constants [11]. This behaviour is tied to the decrease of the lattice parameter with Al^{3+} concentration, that implies an increase of the cohesive force and, consequently, a stiffening of the material.

In spite of our approximation of considering a pure elastic wave propagation we find a weak ($\sim 10^{-3}$) dependence of the phase velocity on the external magnetic field as shown in fig. 4. This result was obtained by measuring the phase difference of the signal and is caused by the ordination of the atomic magnetic moments since the magnetisation curve behaviour is well reproduced.

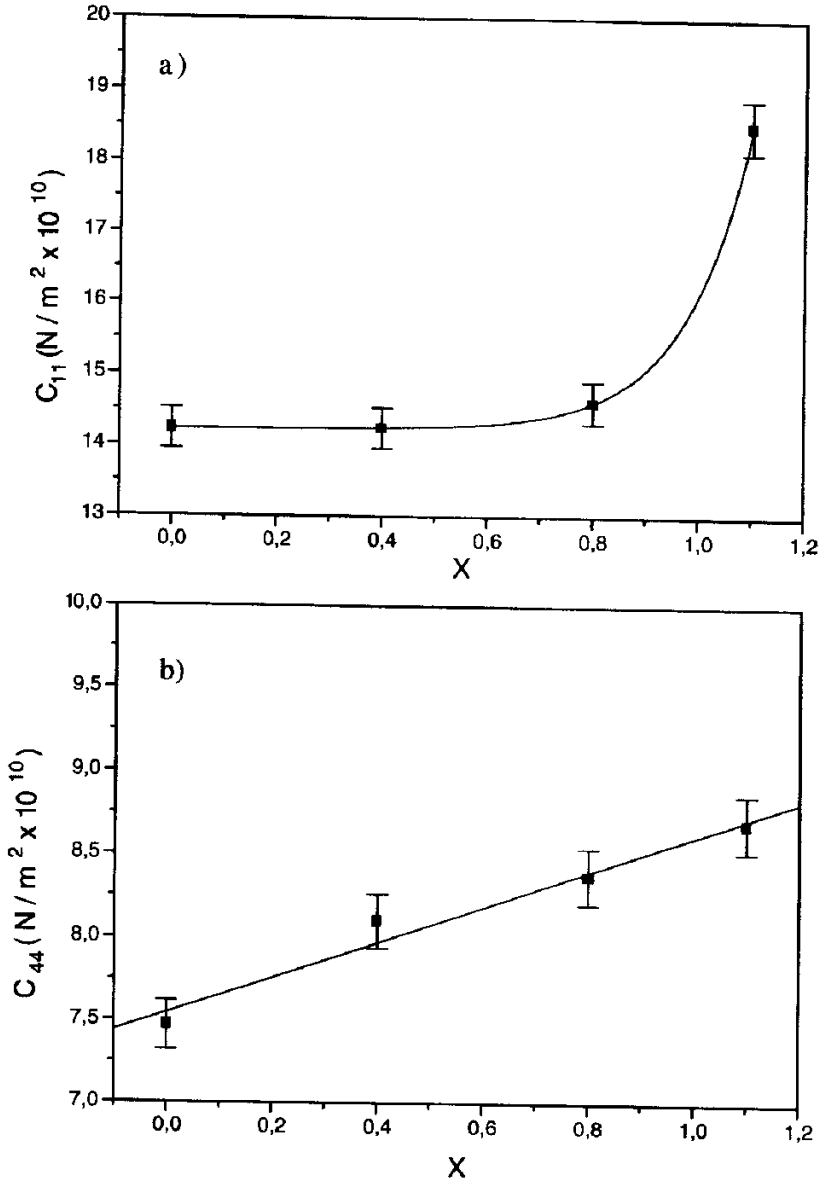

Fig. 3. – Elastic constants C_{11} (a) and C_{44} (b) of $Y_3Fe_{5-x}O_{12}$ *vs.* Al^{3+} concentration.

The decreasing of the lattice parameter with Al^{3+} concentration can explain a cohesive force increment and therefore an increase of phase velocity.

3. – Phonon mean free path

It is well known that the phonon collision includes processes in which a single phonon decays into several, some of which merge into one and so on [12]. It is possible

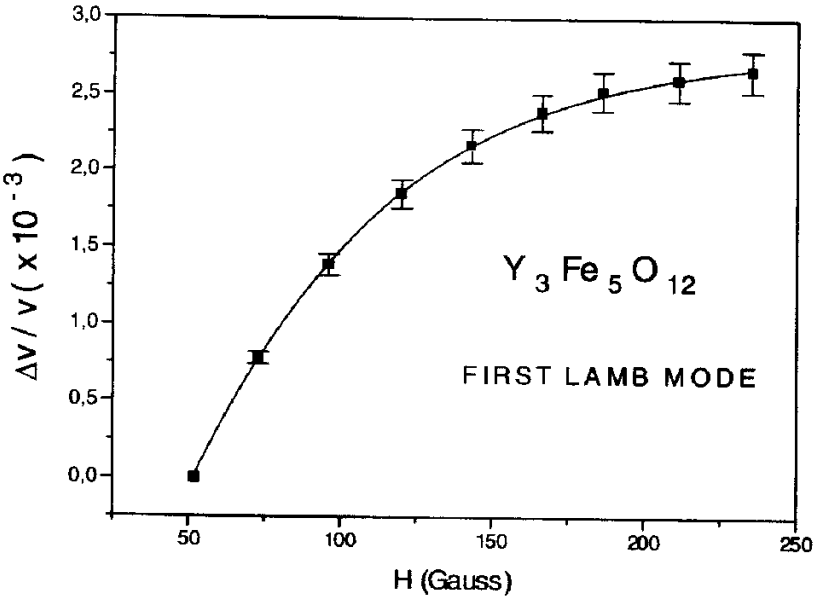

Fig. 4. – Normalised difference of the sound phase velocity in the presence of a magnetic field in the first Lamb mode as a function of the applied field.

to treat the transport of energy by phonons using a Boltzmann equation containing collision terms, and, for a more elementary model, we can introduce a single-phonon relaxation time τ which specifies the probability per unit time of a phonon collision. As in the Drude model, and making use of the Debye approximation, we assume that each phonon will contribute to the thermal current density in the x-direction with an amount equal to the product of the x component of its velocity with its contribution to the energy density which depends on the position of its last collision. In this simple model we assume that the collision occurred at a distance $l = v\tau$ from the point x_0 at which the thermal current is to be calculated in a direction defined from an angle θ to the x-axis.

Phonons with velocity making an angle θ with the x-axis carry an energy density $U(x_0 - l\cos\theta)$ with x-velocity $v\cos\theta$. The net thermal current is proportional to the product of these quantities averaged over all solid angles

$$(13) \qquad j = \int_0^{\pi} v\cos\theta U(x_0 - l\cos\theta)\,\frac{2\pi}{4\pi}\,\mathrm{d}\theta\sin\theta = \frac{1}{3}\,vl\,\frac{\partial U}{\partial T}\left(-\frac{\partial T}{\partial x}\right) = k\left(-\frac{\partial T}{\partial x}\right),$$

where the thermal conductivity k is given as

$$(14) \qquad k = \frac{1}{3}\,cvl\,;$$

here $c = \partial U/\partial T$ is the specific heat of phonons. In a more accurate analysis the

expression of the thermal conductivity is

$$K = \frac{1}{3} \sum_{q,j} c(q,j)\, v(q,j)\, l(q,j), \tag{15}$$

where q is the phonon mode and j is the phonon branch and the sum is over the q values within the first Brillouin zone and over all the branches. The temperature dependence of k is both on c and on the mean free path l.

In order to experimentally evaluate the total phonon mean free path, we can combine the sound velocity value with the thermal diffusivity value obtained on the same samples. From eq. (14) and from the definition of the thermal diffusivity coefficient χ we have

$$k = \frac{1}{3} c v l_{\mathrm{tot}} = \chi c\,, \tag{16}$$

where c is the specific heat, v the sound velocity, l_{tot} is the phonon mean free path and χ is the thermal diffusivity coefficient. By considering the average sound velocity between the longitudinal and share elastic propagation, we obtained the results depicted in fig. 5.

As shown in eqs. (14) and (15), a limiting factor for the thermal conductivity is the phonon mean free path. In fact l depends on many scattering mechanisms. The total phonon mean free path is given by

$$\frac{l}{l_{\mathrm{TOT}}} = \frac{l}{l_{\mathrm{geom}}} + \frac{1}{l_{\mathrm{ph\text{-}ph}}} \tag{17}$$

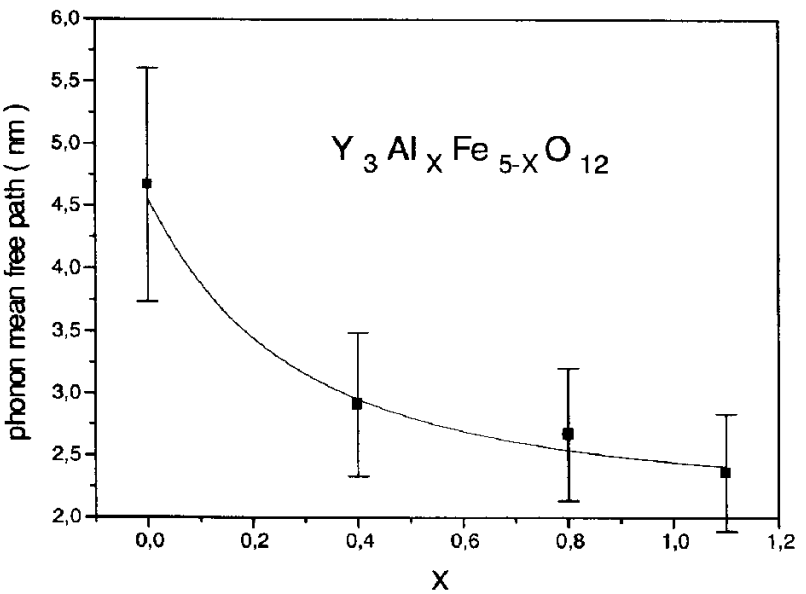

Fig. 5. – Phonon mean free path derived by combining the thermal-diffusivity values with the average sound velocity.

in which the first term is temperature independent and is strongly linked with the sample morphology. In the four granular samples the geometrical disorder seems to be unimportant since the phonon mean free path, depicted in fig. 5, shows a monotonically decay as a function of the Al^{3+} content. This means that porosity and grain boundaries are not linked with phonon scattering since the phonon mean free path is in the order of a few nanometers whilst the mesoscopic disorder size falls in the micrometers range. Moreover the phonon mean free path behaviour observed seems to be linked to the differences in the atomic weight, from the Al^{3+} substitution, resulting in the greatest contribution to unharmonicity of the lattice vibrations and therefore the phonon-phonon interaction term of eq. (17) dominates over the geometrical scattering term.

4. – Conclusions

Thermal-diffusivity measurements and sound velocity measurements over four ceramic YIG materials with substitutions of different amounts of Al^{3+} ions have been carried out. The effects of the magnetic ordering have also been measured both by means of the thermal diffusivity system (evidence of discontinuities corresponding to Neel temperature in a thermal scan) and by means of the ultrasound measurements (ordering of the spin system in a magnetic field sweep). By means of a simple model, in the frame of the kinetic theory, the room temperature phonon mean free path of the four samples has been evaluated using the measured values of the thermal diffusivity and sound velocity. Therefore the complete thermoelastic behaviour of the samples was obtained. From that picture it clearly appears that the phonon mean free path is linked with the differences in the atomic weight of the crystal components, caused by the substitution of the Al^{3+} ions, which give a contribution to the anharmonicity of the lattice vibrations and therefore the phonon-phonon scattering dominates over the geometrical scattering.

REFERENCES

[1] WINKLER G., *Magnetic Garnets* (Friedr. Vieweg, Braunschweig-Wiesbaden) 1981.
[2] LAX B. and BUTTON K. J., *Microwave Ferrites and Ferrimagnetics* (McGraw-Hill, New York) 1962.
[3] SPARVIERI N., PENCO E., SIBILIA C., BERTOLOTTI M., SUBER G. and FERRARI A., *Mater. Lett.*, 5 (1987) 449.
[4] SCHLEMANN E., *J. Appl. Phys.*, 31 (1960) 1647.
[5] TIERSTEN H. F., *J. Appl. Phys.*, 36 (1965) 2250.
[6] STRAUSS W., *Physical Acoustics*, Vol. 4, Part B, edited by W. P. MASON (Academic Press, New York) 1968, pp. 211.
[7] PAREK J. P. and BERTONI H. L., *J. Appl. Phys.*, 44 (1973) 2866.
[8] THOMPSON R. B., *IEEE Trans. On Son. And Ultrason.*, SU-25 (1978) 7.
[9] THOMPSON R. B., *Proceedings of the 1978 Ultrasonic Symposium, Cheng Hill, N.Y., 25-27. Sept. 1978*, edited by J. DE KLERK and B. R. MC AVOY, p. 374.
[10] SOCINO G., SPARVIERI N., TREQUATTRINI F. and VERONA E., *Mat. Chem. Phys.*, 23 (1989) 464.
[11] CLARK A. E. and STRAKNA R. E., *J. Appl. Phys.*, 32 (1961) 1172.
[12] MADELUNG O., *Introduction to Solid State Theory* (Springer-Verlag) 1978.